Monte Carlo simulation of self-avoiding lattice chains subject to simple shear flow. I. Model and simulation algorithm

Guoqiang Xu and Jiandong Ding[a)]
Department of Macromolecular Science, Laboratory of Molecular Engineering of Polymers, Fudan University, Shanghai 200433, China

Yuliang Yang
Department of Macromolecular Science, Laboratory of Molecular Engineering of Polymers, Fudan University, Shanghai 200433, China and Institute of Chemistry, Chinese Academy of Sciences, Beijing 100080, China

(Received 13 March 1997; accepted 3 June 1997)

The efficient on-lattice Monte Carlo (MC) method is extended to simulate, for the first time, the simple shear flow of multiple macromolecular chains with self-avoiding walk (SAW) on a molecular level by introducing a pseudopotential to describe the flow field. This pseudopotential makes sense only for the potential difference associated with each local microrelaxational movement of a bead in the chain strictly defined by the four-site lattice model and bond fluctuation approach. The free-draining bead-spring model is thus investigated at low and high shear rates, and the resultant shear stress and first normal stress difference are obtained by statistics according to the sampled configurational distributions under flow. As the first paper of a corresponding series, the pseudopotential is checked in detail and confirmed by the simulation outputs for both a single SAW chain and multiple SAW chains in two dimensions. The simulated velocity profile is found to greatly satisfy the requirement of the simple shear flow unless the shear rate is unreasonably high. The material functions (apparent viscosity and first normal stress coefficient) show the shear-rate dependence at high shear rate, which is, in turn, explained by the large chain deformation on the microscopic origin. Both Newtonian regime and non-Newtonian regime are found in our on-lattice MC simulation. The nonlinear rheological behaviors at high shear rates revealed in this MC simulation agree with the experimental observations in literature for most polymers. On the other hand, the asymptotic behavior about the chain-length dependence of zero-shear viscosity can be reasonably explained by the present linear viscoelastic theory. Consequently, this paper puts forward a novel and unified simulation approach to study the chain conformation and chain dynamics under shear flow and the nonlinear viscoelasticity of polymeric fluids for both dilute and concentrated solutions or polymer melts. [S0021-9606(97)50334-5]

I. INTRODUCTION

Chain conformation and chain dynamics in various flow fields are long-standing problems of polymer science. Most of the existing theories can only describe the chain behaviors subject to shear or elongation flow within the limitation of linear viscoelasticity and equilibrium problems.[1–3] The other classic problem in chain statistics is about the excluded volume interaction.[4] Even for a single macromolecular chain, the eigenvalue spectrum of a Rouse chain with excluded volume effect is not explicitly known.[5,6] The chain dynamics in the multiple-chain systems is described wonderfully, but merely indirectly, by introducing the tube model reflecting the entanglement effect.[2,3] Due to the inherent difficulties encountered by the analytical theories in dealing with the complicated problems, the computer simulation or computer experiment constitutes a third method between theory and experiment.[7,8] However, the very computer simulations, especially off-lattice approaches, are rather time-consuming, which seriously restricts the scales of the simulated ''real'' time and space. Molecular dynamics simulation[9] and Brownian dynamics simulation[10] of chain conformations under shear flow have been performed during the last decade. Nevertheless, only a single chain is examined. The reason is not the in-principle difficulty, but the unrealistic running time. An efficient simulation approach is thus desired for us to directly mimic the chain conformation and chain dynamics in both single-chain and multiple-chain systems with excluded volume interaction under flow fields, which must shed light into the nonlinear viscoelasticity, non-Newtonian rheological behaviors and nonequilibrium problems for polymers.

Among various simulation approaches, Monte Carlo (MC) simulation, especially the on-lattice approach, distinguishes itself by its high efficiency to describe the dynamics of multiple-chain systems with excluded volume effect.[7] Unfortunately, this method has never been applied to directly simulate even the steady simple shear flow presented as Fig. 1. The inherent difficulty comes from the well-known fact that the prerequisite of performing MC simulation of chain dynamics is to obtain the analytical expressions of all pertinent potentials, and unluckily, the flow-field potentials seem

a)Author to whom correspondence should be addressed.

 0021-9606/97/107(10)/4070/15/$10.00

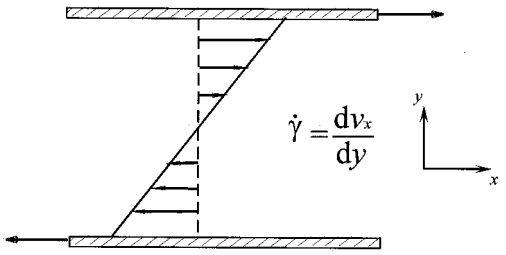

FIG. 1. Schematic presentation of a steady simple shear flow with constant shear rate $\dot{\gamma}$. The geometry and the coordinates are set as marked in the figure. The stagnation line is in the middle between upper and lower slides unless otherwise indicated.

conceptually not to make sense since the simple shear flow corresponds to a dissipative, rotational, and thus nonconservative field.

In order to partly resolve the potential problem, Kramers suggested, over half a century ago, an approach to the calculation of the intrinsic viscosity and other hydrodynamic properties of dilute polymer solutions at low shear rate.[11] This was based on replacing the simple shear flow with the velocity $\mathbf{v}=\dot{\gamma}\, y\mathbf{i}$ ($\mathbf{i}$ Cartesian unit vector in the x direction, $\dot{\gamma}$ shear rate), by its irrotational part, which is derivable from a velocity potential $\phi=0.5\dot{\gamma}\, xy$. According to this potential, the longest relaxation time for a single chain described by the Rouse model, but with excluded volume interaction subject to the Kramers potential flow, was examined by Frisch *et al.*,[12] with the help of MC simulation. In that paper, the self-avoiding walk (SAW) of N steps on a lattice, e.g., the simple-cubic lattice, was generated by MC simulation, and the static configurational distribution function (CDF) under Kramers potential flow was obtained by statistics with this potential as the weighting factor. So the flow process has not been directly mimicked in their simulation. More importantly, most of flow fields achievable in experiment, such as the very popular simple shear flow, can still not be simulated by the MC method.

Recently, a pseudopotential describing the simple shear flow was proposed by us[13] and will be checked in detail in this paper. Although this pseudopotential might not be universal, it does make sense in our MC simulation on the four-site lattice model. This model was first proposed by Carmesin and Kremer,[14] then employed by many others also in zero flow field.[15–18] As the first paper of a corresponding series, the present paper focuses on the model and simulation algorithm, especially the pseudopotential itself. With this pseudopotential put forward by us, the simple shear flow is successfully achieved by the efficient on-lattice MC simulation. Some preliminary results in two dimensions are shown in order to confirm our novel approach. Based on this approach, the equilibrium and nonequilibrium configurations of a single and multiple SAW chains have been studied under simple shear flow. The deformation and orientation of flexible chains at low and moderate shear rates are observed. The shear thinning effect and shear-rate-dependent first normal stress coefficient, which are characteristics of most of the commercial polymers, but absent in the original Rouse model, are revealed. As a result, this work extends, for the first time, the on-lattice dynamic MC simulation into a vivid simulation of the simple shear flow of flexible chains with excluded volume interaction on the molecular level, and obtains, by statistics directly from the simulated CDFs, the macroscopic rheological parameters. This improvement thus affords an efficient method to investigate the nonlinear and nonequilibrium chain dynamics in both dilute solution and in the melt, which is very difficult by present theories or very time consuming by other simulation approaches. This paper does not aim to make more than casual comparisons of our results either to those of other theories or to experiments. Corresponding critical studies would amount to a long communication in itself.

II. MODEL AND POTENTIAL

A. Bond fluctuation algorithm and bead-spring model

As indicated below, the pseudopotential describing the simple shear flow field should be associated with a suitable lattice model and well-defined microrelaxational modes. The most popular choice of lattice model is a generalization of the Verdier–Stockmayer model,[19] where the polymer is represented by a SAW on a simple cubic lattice. Each bond of the SAW should physically correspond to a ''Kuhn segment'' formed by several successive chemical monomers. The simulated behaviors reflect, therefore, the characteristics of chainlike molecules, and the simulated chains stand for the macromolecules rather than oligomers unless they are very short (for instance, less than ten). However, this model has several drawbacks; for instance, the bond length is fixed and the bond angle has only two choices ($0°, \pm 90°$). The alternative algorithm was thus proposed by Carmesin and Kremer.[14] In this bond fluctuation algorithm, one constructs a chain as indicated in Fig. 2. (This figure only represents the two-dimensional counterpart.) In the center of an effective monomer, or strictly say, a bead, four lattice sites on the corner of a square are all blocked for occupation by other beads. The bond vector connecting two successive effective beads may have lengths in the range $l_{\min} \leqslant l \leqslant l_{\max}$. In the four-site model in two dimensions, the length of a Kuhn segment can take six discrete values: 2, $\sqrt{5}$, $\sqrt{8}$, 3, $\sqrt{10}$, and $\sqrt{13}$, and the segment orientation can take 36 discrete angles, as shown in Fig. 2(b). The branching point can also be dealt with [Fig. 2(a)]. According to the choices defined above, not only can two beads not occupy the same lattice, but also the intersection of chains in the course of a sequence of motions is forbidden. So the excluded volume effect is taken into consideration completely. It should be noted that the prototype of the bond fluctuation was first proposed by Larson *et al.* in MC simulation of amphiphile–oil–water systems and called chain twisting.[20] However, the conventional single-site model was used there, and the bond length can only take two discrete values, 1 and $\sqrt{2}$, which is not sufficient for the problem encountered in the present paper.

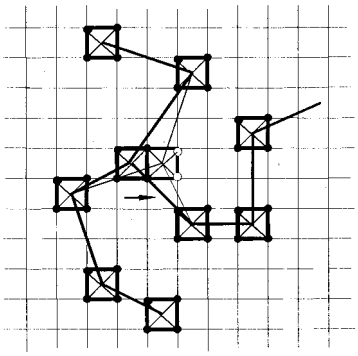

(a)

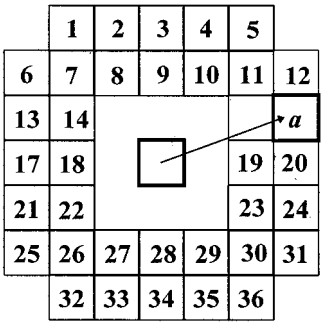

(b)

FIG. 2. (a) Schematic presentation of the four-site model and bond fluctuation algorithm; (b) a single dimer $A-B$, demonstrating the restriction of the bond length or segment length l to $2 \leqslant l \leqslant \sqrt{13}$ for the two-dimensional case. Assuming monomer or bead A on the plaquette in the center, bead B can occupy 1 of the 36 allowed plaquettes, which are labeled by numbers a from $a=1$ to $a=36$.

The fluctuation of the length of the bond vector can be comprehended as that of the length of the physical Kuhn segment. A harmonic elastic energy is thus introduced associated with the bond fluctuation,

$$U_{\mathrm{el}} = \tfrac{1}{2} H (l - l_0)^2, \tag{1}$$

where H is the corresponding elastic constant and l_0 is the equilibrium length. Similar elastic energies were put forward by Binder *et al.* to study the polymer glass transition by MC simulation based on the bond fluctuation algorithm,[16,17] where l_0 is taken as $l_{\max}$ and H is an adjustable parameter. That is very nice to solve the problem in corresponding references.[16,17] However, the parameters l_0 and H should have their specific definitions in this paper. Since the so-called bond actually refers to a Kuhn segment, the bond length fluctuation energy comes, in our understanding, from Brownian motion and reflects the restoring energy due to deviation of the CDF of the monomers within one Kuhn segment from the most probable distribution. The l_0 must be zero and H denotes the elastic constant of the ''entropy spring'' expressed as

$$l_0 = 0, \tag{2a}$$

$$H = kTK, \tag{2b}$$

$$K = 2b^2, \tag{2c}$$

where kT is the Boltzmann constant times the absolute temperature, b is the parameter describing the CDF under approximation of Gaussian distribution, with the distribution function $W(x,y)$ or $W(x,y,z)$ written as

$$W = \left(\frac{b}{\sqrt{\pi}} \right)^d e^{-b^2 l^2}. \tag{3}$$

In Eq. (3), d is the dimensionality. The parameter b is related to the most probable segment length l^* as

$$b^2 = \begin{cases} \dfrac{1}{2l^{*2}} & (d=2) \\ \dfrac{1}{l^{*2}} & (d=3) \end{cases} \tag{4}$$

in two and three dimensions, respectively. Hence, the four-site model can be regarded as a bead-spring model. Following the Rouse model, the polymer molecule is divided up into $N-1$ equal submolecules (Kuhn segments). Each submolecule is a portion of polymer chain just long enough so that at equilibrium the separation of its ends obeys, to a first-order approximation, a Gaussian probability function. Then the polymer molecule is considered to be replaced by a chain of N identical beads joined by $N-1$ flexible spring segments.

Compared to the Rouse model,[5] the spring in the four-site model can not be infinitely stretchable and somehow similar to the Tanner spring[21] or a ''linear locked'' spring with the restriction of $l_{\min} \leqslant l \leqslant l_{\max}$. We reasonably set the most probable segment length as

$$l^* = \tfrac{1}{2}(l_{\min} + l_{\max}). \tag{5}$$

If the monomer configurational distribution within one Kuhn segment is Gaussian, the mean segment length and the root mean square segment length are also located between $l_{\min}$ and $l_{\max}$ considering the concrete values of $l_{\min}$ and $l_{\max}$ in this case. So, the restriction of segment length does not bring about severe deviation of the present model from the Rouse model. However, in the original Rouse model, the excluded volume effect is not taken into consideration at all. The Zimm model has, together with treating hydrodynamics interaction, considered partly the excluded volume effect in preaveraging the Oseen–Burgers tensor by revising the static scaling exponent.[3] But, the intersection of chains in the course of a sequence of motions is still permissible and the dynamics in the multiple-chain system, e.g., entanglement effect, can not be dealt with in the conventional Rouse–Zimm formalism. The improvement of the Rouse model with excluded volume effect in the present paper is hence nontrivial. Although the hydrodynamics interaction is disregarded by the lattice model, it is nevertheless of interest to clarify the behaviors in the limit where such hydrodynamic effects can be neglected, especially in the bulk state. The tested model in this paper is, therefore, a free-draining bead-spring model with excluded volume effect.

One of the advantages of the four-site model is that since the bond length can be altered, the conventional microrelaxational modes in MC simulation, such as the end bond rotation, kink jump motion, and 90° crankshaft rotation on the simple cubic lattice[19] are unnecessary. It is sufficient to consider merely one type of move as depicted in Fig. 2, namely the random jump of an effective bead in a random chosen lattice direction by a lattice unit. The coordination number of the lattice directions is 4 or 6 in two and three dimensions, respectively. For each trial, and thus each local movement, the coordinates of x, y, and z can only be varied in one of them, which is crucial for the pseudopotential describing the simple shear flow given in the subsequent paragraphs.

In dynamic MC simulation of a thermodynamic system, the Metropolis[22] or Glauber dynamics[23] transition probability,

$$P_{\mathrm{Me}}=\min\{1,\exp[-\Delta E/(kT)]\}, \tag{6a}$$

$$P_{\mathrm{Gl}}=\frac{\exp[-\Delta E/(kT)]}{1+\exp[-\Delta E/(kT)]} \tag{6b}$$

can be employed for accepting or rejecting a move, which is allowed according to the excluded volume and segment length restrictions. The transition probabilities involve an energy change ΔE between the new (trial) and old states. It has been demonstrated that the probability in a Metropolis importance sampling obeys the master equation for a Markov stochastic process, and therefore, the MC time t in the unit of MC cycle t_{MC} embodies the real time with a constant proportion coefficient.[7] The Glauber dynamics sampling can also be used to mimic the chain dynamics due to the same reason, although it is not as popular as the Metropolis sampling.

B. Pseudopotential for the simple shear flow

If a particle moves in a flow field, the force exerted on the particle by the flow field can, after neglecting the hydrodynamics interaction and inertial effect, be expressed as

$$\mathbf{f}_m=\xi\boldsymbol{\nu}=\xi\nabla U_\nu, \tag{7}$$

where ξ is the friction coefficient and assumed to be a constant, and U_ν is the velocity potential. By the virtual-work principle, the flow-field force can be obtained by the derivative of the flow-field potential U_s as

$$\mathbf{f}_m=-\nabla U_s. \tag{8}$$

So

$$U_s=-\xi U_\nu=-\frac{kT}{D}U_\nu, \tag{9}$$

where D is the diffusivity.

It is well known that the simple shear flow can be divided into two parts:

$$\boldsymbol{\nu}=\dot\gamma y\mathbf{i}=\tfrac{1}{2}\dot\gamma(y\mathbf{i}+x\mathbf{j})+\tfrac{1}{2}\dot\gamma(y\mathbf{i}-x\mathbf{j}). \tag{10}$$

The former is a purely elongational flow and named conventionally as the Kramers potential flow since it can be rewritten as $0.5\dot\gamma\nabla(xy)$, and thus the Kramers potential reads $U_{\mathrm{Kr}}=0.5\xi\dot\gamma xy$; the latter is a purely rotational flow and the flow-field potential does not make sense since the corresponding field involves vortex. Consequently, the flow field for the simple shear flow is not conservative. The potential difference between two points in a simple shear flow depends, in fact, on the concrete routes between these two points (x_1,y_1,z_1) and (x_2,y_2,z_2) or $(x_1+\Delta x,y_1+\Delta y,z_1+\Delta z)$. However, the potential difference is definite if we define the specific route for every microrelaxation step. In the MC simulation on square or cubic lattice, especially for the four-site model, every microrelaxation step for a segment, or generally speaking, a particle or a bead in the Rouse model, should be satisfied with Δx, Δy, $\Delta z=0,\pm1$ and the Δx, Δy, and Δz can not take nonzero values simultaneously since any cooperative relaxation modes are forbidden. Along the well-defined route in this course-grained lattice model, we can tentatively write down the total differential of the potential of flow field, dU_s. Since

$$\nabla U_s=\frac{\partial U_s}{\partial x}\mathbf{i}+\frac{\partial U_s}{\partial y}\mathbf{j}+\frac{\partial U_s}{\partial z}\mathbf{k}=-\frac{kT}{D}\dot\gamma y\mathbf{i}, \tag{11}$$

we can get

$$\frac{\partial U_s}{\partial x}=-\frac{kT}{D}\dot\gamma y,\quad \frac{\partial U_s}{\partial y}=\frac{\partial U_s}{\partial z}=0. \tag{12}$$

So

$$dU_s=\frac{\partial U_s}{\partial x}dx+\frac{\partial U_s}{\partial y}dy+\frac{\partial U_s}{\partial z}dz=-kT\Gamma y\,dx, \tag{13}$$

where Γ is the reduced shear rate in the unit of l_{MC}^{-2} (l_{MC}, the unit lattice size in MC simulation, is set to be 1 as usual) and reads

$$\Gamma=\dot\gamma/D. \tag{14}$$

The potential difference for a particle moving from (x_1,y_1,z_1) to (x_2,y_2,z_2) is thus described as

$$\Delta U_s=-kT\Gamma\int_{x_1}^{x_2}y\,dx=\tfrac{1}{2}kT\Gamma(x_1-x_2)(y_1+y_2)$$
$$=\begin{cases}0 & (\Delta x=0,\Delta y\ \text{ or }\ \Delta z=\pm1)\\ \mp kT\Gamma y & (\Delta x=\pm1,\Delta y\ \text{ or }\ \Delta z=0)\end{cases}. \tag{15}$$

This equation is valid in both two dimensions and three dimensions.

At this stage, it is absolutely necessary to give some comments to the expression of the potential of simple shear flow field [Eq. (15)]. First, we just describe a pseudopotential for the simple shear flow because the flow fields, except Kramers potential flow, are not conservative and the concept of potential does not make sense. In fact, Eq. (15) is not a strict derivation result since the conditions of the total differential dU_s [Eq. (13)] are not satisfied completely. So, Eq. (15) should be confirmed by the simulation outputs. Second, Eq. (15) only expresses the *pseudopotential difference* between two nearest-neighbor (NN) positions achievable in a minimum local microrelaxational mode in the course-grained lattice model, rather than the pseudopotential itself, because

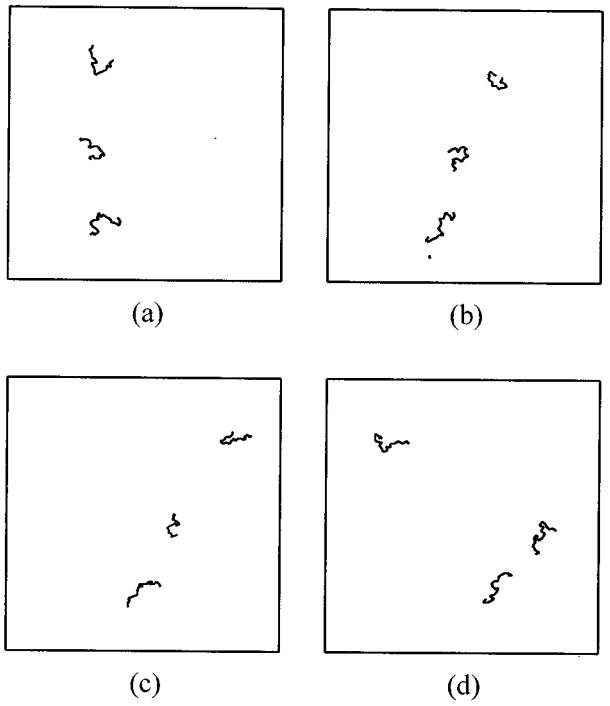

FIG. 3. Typical snapshots of three chains in the simulated shear flow in time sequence, especially showing the velocity gradient along the dimension perpendicular to the shear flow. The periodic boundary condition is used along the x direction whereas the y direction is restricted by two hard walls. The number of beads $N=20$; the system size $L_x \times L_y = 200 \times 200$ with the stagnation point located at the lower boundary; the input reduced shear rate $\Gamma = 0.002$.

we can not set a fixed point as zero potential. Fortunately, in MC simulation based on Metropolis sampling or Glauber dynamics sampling, only the energy difference for every local microrelaxational movement is required [Eqs. (6a) and (6b)]. It is very lucky that the expression of the pseudopotential put forward by us [Eq. (15)] is valid in on-lattice MC simulation when the four-site lattice model and the associated local microrelaxational mode are employed after combination of the Metropolis or Glauber dynamics importance sampling method. It should be difficult, if not impossible, to extend the analytical expression of the pseudopotential of the flow field, Eq. (15), to the other cases.

III. SIMULATION OUTPUTS OF THE PSEUDOPOTENTIAL FLOW FIELD

In the subsequent sections, we will examine the simulation outputs to confirm the pseudopotential describing the simple shear flow of the macromolecular chains. Only the results in two dimensions are presented in this paper. The most important question we should address is whether or not the simple shear flow can be achieved by the pseudopotential put forward above. A series of snapshots in the simulated shear flow are shown in Fig. 3. Obviously, the simulated chains move along the x or horizontal direction and there is a velocity gradient along the y or perpendicular direction. However, the quantitative analysis should be made to further analyze and confirm the pseudopotential.

A. Metropolis sampling and Glauber dynamics sampling

First, we would like to give an analysis of the velocity and then the velocity gradient achieved in our on-lattice MC simulation. For every bead, the average flow velocity along the x direction in our MC simulation can be expressed as

$$\nu_x = N_x(P_1 - P_2) l_{\mathrm{MC}}/t = C(P_1 - P_2), \tag{16}$$

where P_1 and P_2 stand for the probabilities for forward and backward jumps, respectively, t is the MC time, N_x is the number of forward or backward trial jumps along the x direction which do not violate SAW and bond length restriction, $C = N_x l_{\mathrm{MC}}/t$, denoting the lattice length times the number of forward or backward trial jumps per MC circle. The unit of ν_x is thus $l_{\mathrm{MC}}/t_{\mathrm{MC}}$, where t_{MC} is the unit time in MC simulation referring to the MC time during which every bead in the system is tried once. The value of velocity depends upon the concrete course-grained model and also upon the sampling methods.

For the Metropolis sampling method,

$$P_1 = 1, \quad P_2 = e^{-\Gamma y}. \tag{17}$$

So the flow velocity reads

$$\nu_x = C_{\mathrm{Me}}(1 - e^{-\Gamma y}). \tag{18}$$

Then, we can obtain the shear rate as

$$\dot{\gamma}_{\mathrm{Me}} = \frac{d\nu_x}{dy} = C_{\mathrm{Me}} \Gamma e^{-\Gamma y} = \begin{cases} C_{\mathrm{Me}}\Gamma & (\Gamma y \to 0) \\ 0 & (\Gamma y \to \infty) \end{cases}. \tag{19}$$

The unit of the shear rate is t_{MC}^{-1}. When $\Gamma y \ll 1$, the zeroth-order approximation of the Taylor series of $\exp(-\Gamma y)$ gives

$$\dot{\gamma}_{\mathrm{Me}} = C_{\mathrm{Me}}\Gamma = \text{constant}. \tag{20}$$

This is a typical expression of the simple shear flow.

Alternatively, for Glauber dynamics sampling, the probabilities of forward and backward jumps become

$$P_1 = \frac{e^{\Gamma y}}{1 + e^{\Gamma y}}, \quad P_2 = \frac{e^{-\Gamma y}}{1 + e^{-\Gamma y}}. \tag{21}$$

Then the flow velocity of a bead reads

$$\nu_x = C_{\mathrm{Gl}} \frac{1 - e^{-\Gamma y}}{1 + e^{-\Gamma y}} = C_{\mathrm{Gl}} \,\mathrm{th}\left(\frac{1}{2}\Gamma y\right). \tag{22}$$

The corresponding shear rate is thus

$$\dot{\gamma}_{\mathrm{Gl}} = \frac{1}{2} C_{\mathrm{Gl}}\Gamma \,\mathrm{sech}^2\left(\frac{1}{2}\Gamma y\right) = \frac{2C_{\mathrm{Gl}}\Gamma e^{-\Gamma y}}{(1 + e^{-\Gamma y})^2}$$

$$= \begin{cases} \frac{1}{2}C_{\mathrm{Gl}}\Gamma & (\Gamma y \to 0) \\ 0 & (\Gamma y \to \infty) \end{cases}. \tag{23}$$

When $\Gamma y \ll 1$, both the zeroth-order and first-order approximation of the Taylor series of $\exp(-\Gamma y)$ give

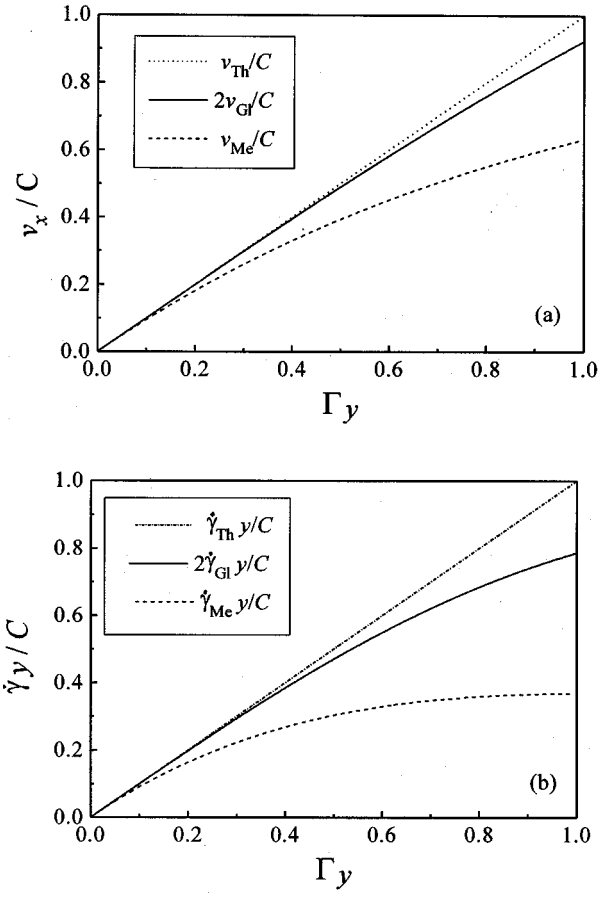

FIG. 4. (a) The reduced velocity of the simple shear flow, v_x/C, as a function of Γy, the reduced shear rate times y coordinate. v_{Th} denotes the theoretical flow velocity for an ideal simple shear flow with $v_{Th}=C\Gamma y$, while v_{Gl} and v_{Me} result from the analysis of Glauber dynamics sampling [Eq. (22)] and Metropolis sampling [Eq. (18)], respectively. (b) The reduced output shear rate $\dot{\gamma}/C$ times y coordinate as a function of Γy. $\dot{\gamma}_{Th}=C\Gamma$ while $\dot{\gamma}_{Gl}$ and $\dot{\gamma}_{Me}$ are expressed by Eqs. (23) and (19), respectively.

$$\dot{\gamma}_{Gl}=\tfrac{1}{2}C_{Gl}\Gamma=\text{constant}, \tag{24}$$

which results in the simple shear flow also.

The simulation outputs show that

$$C_{Me}=C_{Gl}=C, \tag{25}$$

which clearly indicates that the different sampling methods alter only the transition probabilities [Eqs. (6a) and (6b)]. C is determined by the SAW properties and bond length restrictions. For a separated single bead in a dilute solution, C takes the maximum and equals $1/(2d)$, where $2d$ is the coordination number. Hence when $\Gamma y \ll 1$,

$$v_{Gl}=\tfrac{1}{2}v_{Me}, \tag{26a}$$

$$\dot{\gamma}_{Gl}=\tfrac{1}{2}\dot{\gamma}_{Me}=\tfrac{1}{2}C\Gamma. \tag{26b}$$

These results can also be seen from the calculation according to Eqs. (18), (19), (22), and (23) (see Fig. 4).

As a result, both Metropolis sampling and Glauber dynamics sampling can be employed to simulate the simple shear flow on lattice. Metropolis dynamics is faster than Glauber dynamics and exhibits twice the evolution velocity

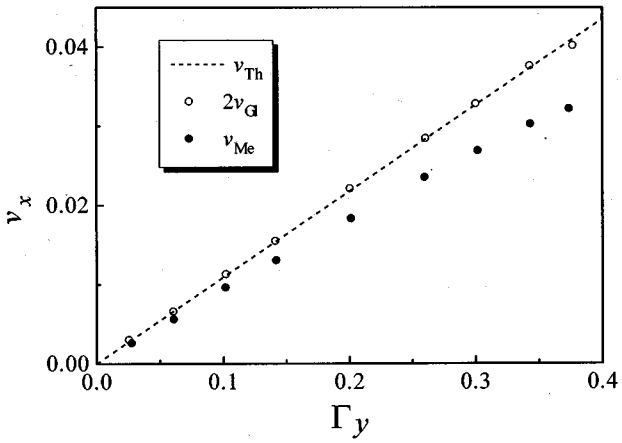

FIG. 5. The simulated flow velocity v_x for a single chain as a function of Γy. v_{Th} denotes the theoretical flow velocity for an ideal simple shear flow with $v_{Th}=C\Gamma y$ ($C=0.11$) while v_{Gl} and v_{Me} are MC simulation outputs resulting from the Glauber dynamics sampling and the Metropolis sampling, respectively. $N=20$. $L_x\times L_y=200\times 200$. For every point, the statistics is initiated after evolution for 1000 MC cycles at given shear rate. The ensemble average over 100 independent runs is performed, and for each run the time average over 10 000 MC cycles is made.

at low shear rate [Eqs. (26a) and (26b)]. However, the linear range of the output flow velocity for Metropolis sampling is narrower than that of Glauber dynamics, which can be seen from theoretical analysis (Fig. 4) and also from the simulation outputs of a single chain subject to the pseudopotential flow (Fig. 5). We would like to mention that the simulated flow velocity is, in principle, not a linear, but an exponential function of the y coordinate [Eqs. (18) and (22)], just similar to the original expression of Rouse theory [Eq. (1) in Ref. 5]. So, the simulated shear rate can not be regarded as a linear function of the y coordinate, unless the flow velocity is sufficiently small. The constant velocity gradient along the normal direction of flow, which is the characteristic of the simple shear flow, can only be achieved when $\Gamma y \ll 1$ under zeroth-order approximation for Metropolis sampling [Eq. (20)] or under first-order approximation for Glauber dynamics simulation [Eq. (24)]. Consequently, we prefer Glauber dynamics to Metropolis sampling in order to achieve a relatively higher shear rate in the simple shear flow simulated by our on-lattice MC method. In the following sections all simulated results are the outputs of Glauber dynamics simulation.

B. Velocity profile of simulated flow field

Now we check whether or not the steady laminar flow and constant shear rate can be achieved in our MC simulation based on the four-site, course-grained lattice model and corresponding pseudopotential describing the simple shear flow. A single chain with the number of beads $N=20$ is taken as an example. For every independent run, the center of mass of the chain is located at one point, with fixed y coordinate at the initial state. The average displacement along the x direction is recorded and plotted versus simulation shear time (Fig. 6). Since the thermal fluctuation, and

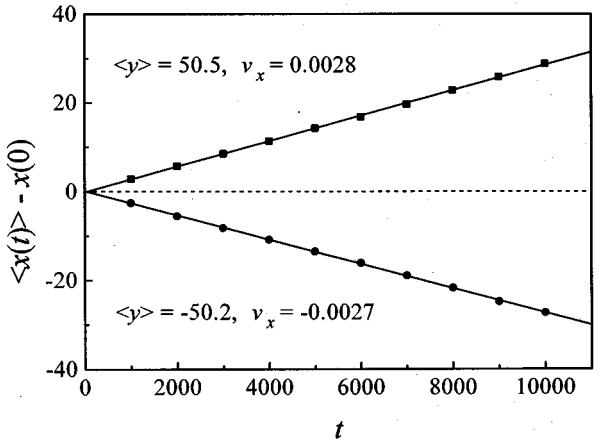

FIG. 6. The average displacement along the flow direction $\langle x(t)\rangle - x(0)$ for a single chain plotted versus simulation shear time t in the unit of attempted MC step per bead, t_{MC}. For every independent run, the center of mass of the chain is located at $y=50$ or -50 at the initial state. The velocity $v_x(y)$ can be obtained from the slope of the corresponding straight line. ($\Gamma=0.001$; the other parameters are the same as those in Fig. 5.)

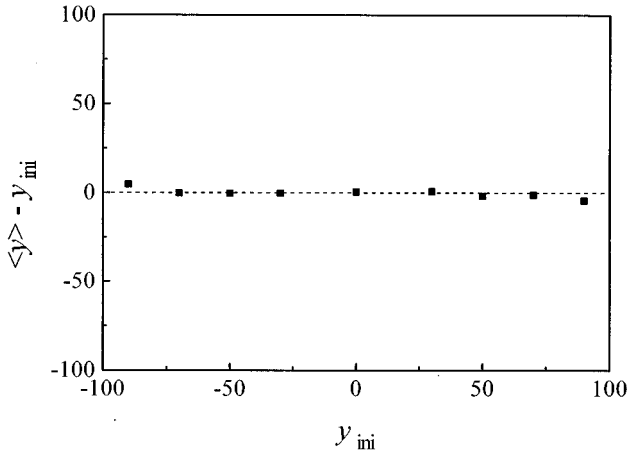

FIG. 8. The average displacement $\langle y\rangle - y_{\mathrm{ini}}$ at different initial positions along the velocity gradient direction. ($\Gamma=0.001$; the other parameters are the same as those in Fig. 5.)

thus the diffusion process, has been embodied in the Metropolis or Glauber dynamic sampling to the microrelaxational movements, the friction is implicitly involved in the dynamic MC simulation. So, there is no inertial, and thus accelerating, mechanism in the present simulation. It is obvious that the simulated flow is a steady laminar flow. The flow velocity v_x can be readily obtained from the slope of the line $\langle x(t)\rangle - x(0)$ versus t. Since the stagnation point is defined in the middle ($y=0$) as shown in Fig. 1, the velocities for positive and negative ys exhibit opposite signs (Fig. 6).

Although the averaged flow velocity does not change with the running time, it varies with different positions along the normal direction of the flow velocity. A linear relation of velocity to y coordinate is clearly shown in Fig. 7. From the slope of this straight line, the velocity gradient or the shear rate can be obtained directly. The simple shear flow is achieved in our on-lattice MC simulation according to the pseudopotential.

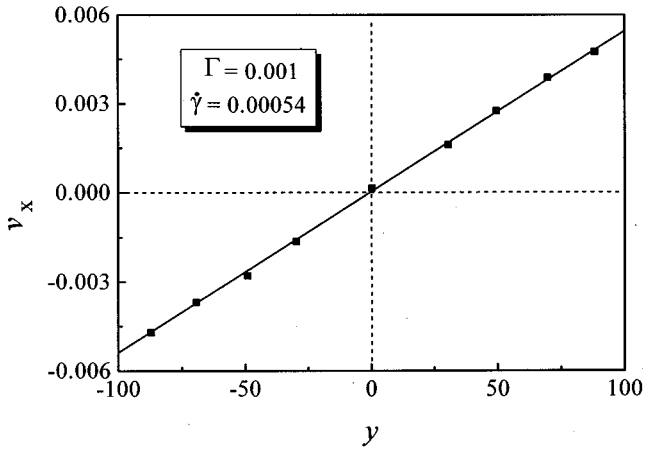

FIG. 7. Simulated flow velocities at different positions along the dimension of velocity gradient. The simulated shear rate $\dot{\gamma}$ in the unit of t_{MC}^{-1} is obtained from the slope of this straight line and might be different from the input reduced shear rate Γ in the unit of l_{MC}^{-2}. (The simulation parameters are the same as those in Fig. 5.)

The lattice system is defined as the y direction restricted by hard walls, while the periodic boundary condition is applied along the x direction. Therefore, it should be noted that near the upper and lower boundaries the ensemble-averaged displacement along the y direction may deviate from zero (see Fig. 8, where y_{ini} is the initial position and $\langle y\rangle$ is the ensemble average of the y values after evolution for sufficiently long MC time). This clearly shows that the chain may be bounced back at the hard wall in the course of shear flow. Nevertheless, at most of the positions, the displacements along the y direction are nearly zero (Fig. 8) and not influenced by the boundaries. The on-lattice simulation is, therefore, valid for macromolecular chains only if the gap length between upper and lower boundaries is several times the radius gyration of the chain, unless we just pay attention to the constrained conformation of the macromolecular chains under shear flow.

IV. FLOW-INDUCED CHAIN DEFORMATION

The configuration of a chain described by the four-site model has been investigated in detail by us. The results in zero field will be published in another paper.[24] Reasonably, the simulated mean square radius of gyration S_G^2 obeys the conventional static scaling law[4] as $S_G^2 \propto (N-1)^{2\nu}$, where the exponent ν equals 3/4 for a single SAW chain in two dimensions, but nearly 1/2 in the concentrated solution with the occupied volume fraction $\varphi > 0.5$.

Besides the chain size, the chain shape is also very important, which can be described by the second-rank tensor of radius of gyration, $\hat{\mathbf{S}}$. If the position of the ith bead in a chain with N beads is located at $\mathbf{r}_i=(x_i,y_i)$ $(i=1,2,...,N)$ with respect to the center of gravity, the tensor of radius of gyration is written as

$$\hat{\mathbf{S}}=\frac{1}{N}\begin{bmatrix}\sum_{i=1}^{N}x_i^2 & \sum_{i=1}^{N}x_iy_i\\ \sum_{i=1}^{N}y_ix_i & \sum_{i=1}^{N}y_i^2\end{bmatrix}=\begin{bmatrix}S_x^2 & S_{xy}\\ S_{yx} & S_y^2\end{bmatrix}, \tag{27}$$

where S_x^2 and S_y^2 denote the xx and yy components of the tensor of radius of gyration. The trace of matrix gives the scaled radius of gyration

$$S_G^2=\mathrm{Tr}\ \hat{\mathbf{S}}=S_x^2+S_y^2. \tag{28}$$

Therefore, S_x^2 and S_y^2 also mean the x and y components of the scaled radius of gyration, where x and y dimensions are, in the present paper, parallel with the directions of shear flow and velocity gradient, respectively. The symmetry matrix with $S_{xy}=S_{yx}$ can be, by a suitable triangle matrix $\hat{\Lambda}$, diagonalized as

$$\hat{\Lambda}\hat{\mathbf{S}}\hat{\Lambda}^{-1}=\begin{bmatrix}\lambda_1 & 0\\ 0 & \lambda_2\end{bmatrix}. \tag{29}$$

The eigenvalues λ_1 and λ_2 correspond to the square lengths of the two principal axes if the chain shape is regarded as an ellipse, and can be expressed analytically as:

$$\lambda_{\max}=\max(\lambda_1,\lambda_2)=\tfrac{1}{2}S_G^2+\lambda', \tag{30a}$$

$$\lambda_{\min}=\min(\lambda_1,\lambda_2)=\tfrac{1}{2}S_G^2-\lambda', \tag{30b}$$

where

$$\lambda'=\sqrt{\tfrac{1}{4}(S_x^2-S_y^2)^2+S_{xy}^2}. \tag{30c}$$

The eigenvector associated with the maximum eigenvalue, $\mathbf{n}$, gives the orientation angle of the long principal axis of the ellipse with

$$\mathrm{tg}\ \Theta=\frac{\lambda'-0.5(S_x^2-S_y^2)}{S_{xy}}. \tag{31}$$

The degree of the coil anisotropy can be described by the order parameter, O,

$$O=\frac{2}{S_G^2N}\sum_{i=1}^{N}(\mathbf{r}_i\cdot\mathbf{n})^2-1=\frac{2\lambda_{\max}}{S_G^2}-1=\frac{|\lambda_1-\lambda_2|}{\lambda_1+\lambda_2}, \tag{32}$$

with $O\in[0,1]$. $O=0$ and $O=1$ correspond to a sphere and a rod, actually.

In zero field, the chain configuration is isotropic in the laboratory frame. Hence, the orientation order parameter O obtained from this tensor must be zero and the orientation angle Θ loses its definition. However, the chain may be deformed and oriented subject to shear flow, and under relatively high shear rate, nonlinear deformation of chain configuration may occur, which is rather difficult to describe analytically, but is convenient to reveal by our on-lattice MC simulation.

A. Dynamics behavior: Chain tumbling under simple shear flow

Figure 3 has shown the chain movement along the flow direction and a velocity gradient along the perpendicular direction. The chain configuration is simultaneously changed in the process of flow. In order to show clearly the chain dynamics under a simple shear flow, we examine a longer single chain with $N=80$, and show a series of snapshots in the center-of-gravity coordinate system (Fig. 9). The zero orientation angle is defined as along the flow direction. It is interesting that the principal axis of the tensor of radius of gyration is rotated continuously and in a statistic sense, clockwise in the geometry defined by Fig. 1. This phenomenon reminds us of the director tumbling of liquid crystals (LCs), especially the main-chain LC polymers subject to simple shear flow, if they have a positive third Leslie coefficient.[25,26] More complicated than the rigid macromolecules, the flexible chain is elongated during tumbling, especially when the transient principal axis is located nearly along $\pi/4$ (Fig. 9).

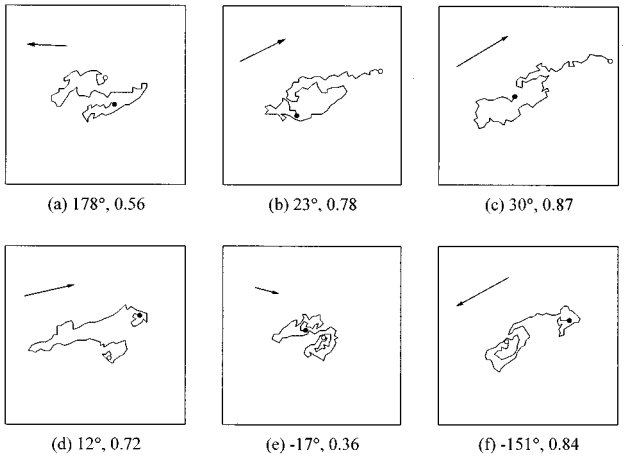

FIG. 9. Typical snapshots of a single chain in dilute solution under the simulation simple shear flow in time sequence. The rotation and deformation of the chain are especially shown, while the displacement of center of gravity is not. The orientation angle Θ and the order parameter O obtained from the tensor of the radius of gyration are indicated below each snapshot. The direction and length of each marked arrow refer to the corresponding Θ and O, respectively. In order to show the chain tumbling more clearly, the chain ends are marked with the open circle and solid circle. ($N=80$; $L_x\times L_y=200\times200$; marked-box size: 100×100; $\Gamma=0.002$; the initial center of gravity of this chain is located at the center of the lattice system.)

These dynamic behaviors of a flexible chain under shear flow can be shown by Eq. (10), in which the simple shear flow is divided into a purely elongational flow and a purely rotational flow. The vortex involved in the simple shear flow results in the chain rotation. If we describe the position of the bead in the center-of-gravity coordinate system as $x=l\cos\theta$ and $y=l\sin\theta$, the velocity potential of rotation flow can be formally, not strictly, written as $\Delta u_{\nu,\mathrm{rot}}=-0.5\dot{\gamma}l^2\Delta\theta$. That describes a monotonous rotation (clockwise), which accounts for tumbling. On the other hand, the Kramers potential can be rewritten as $\Delta u_{\nu,\mathrm{Kr}}=0.25\dot{\gamma}l^2\sin(2\theta)$. That describes an elongational flow along $\pi/4$, which accounts for the deformation and orientation of flexible chain along with tumbling. Similar phenomena about the stretching and rotation of a single chain under steady

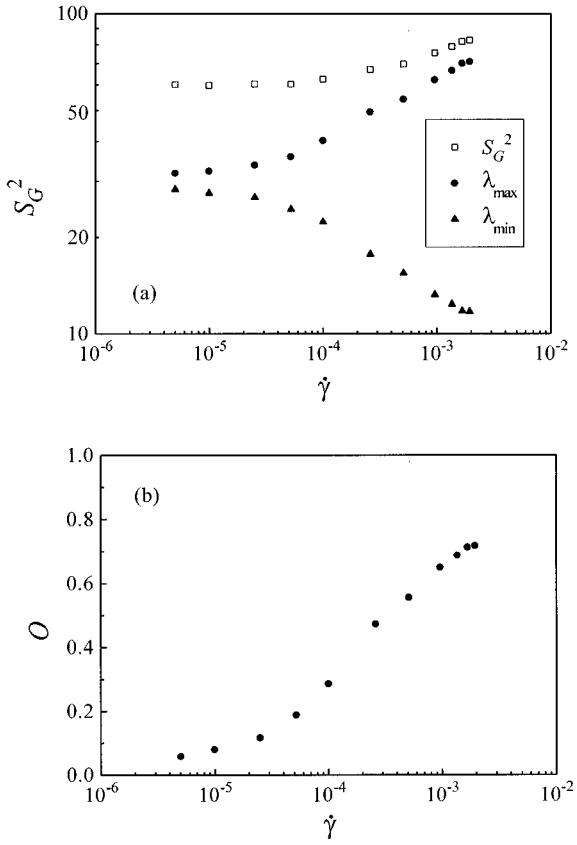

FIG. 10. (a) Mean square radius of gyration, S_G^2 and its principal components, λ_{max} and λ_{min}, and (b) order parameter O as a function of shear rate $\dot{\gamma}$. ($n_p=20$; $N=80$; $L_x\times L_y=100\times 100$; so $\varphi=0.16$; 10 independent runs are averaged and for each run, 10 000 MC cycles are averaged after 10 000 MC cycles under shear.)

shear flow were observed in Brownian dynamics simulation.[10]

B. Steady-state behavior: Chain stretching and orientation under flow

Equation (27) refers to a single chain at any time. Thus, Eqs. (28), (32), and (31) describe the transient chain size, chain shape, and chain orientation, respectively. If the average is performed over different times, different ensembles, or different chains in the course of the statistics of the tensor of radius of gyration [Eq. (27)], Eqs. (28), (32), and (31) then give the mean chain configuration for a single chain or multiple chains. Since at different times or in different ensembles the chain tumbles in different phases, the tumbling behavior for a single chain is suppressed after time average or ensemble average. Compared to this, the chain deformation and orientation are still very striking. The cases for a single chain and multiple chains are likewise.

Figure 10 shows the dependence of radius of gyration, S_G^2, and order parameter O upon shear rate $\dot{\gamma}$. A multiple-chain system is simulated with the occupied volume fraction $\varphi=0.16$. The chains are apparently elongated since the long principal axis, λ_{max}, gets longer and longer with the shear rate increased, whereas the short principal axis, λ_{min}, gets shorter and shorter [Fig. 10(a)]. The global chain size, i.e., the radius of gyration, increases with shear rate also. The elongation is pronounced considering the large order parameter at relatively high shear rate [Fig. 10(b)]. A continuous transition can furthermore be observed in Figs. 10(a) and 10(b), by which, the flow field can be roughly divided into low shear rate regime and medium or high shear rate regime; in other words, the macroscopic behaviors can be roughly divided into linear and nonlinear regimes. It is very good that the pseudopotential put forward in this paper can be employed to investigate the nonlinear viscoelastic and rheological behaviors of chainlike molecules, albeit the limit $\Gamma y \ll 1$ should be satisfied in order to meet the requirement of the simple shear flow with a constant velocity gradient.

It is necessary to indicate that with the shear rate increased, the averaged segment length or bond length in our model changes only slightly, whereas the whole chain is stretched dramatically. The deformation of a flexible chain is thus mainly reflected by that of the global CDF and is insensitive to the detail in the short length-scale for the course-grained model. The validity of the present bead-spring model relies on the assumption of Hookean spring for each Kuhn segment, which originates from the Gaussian argument to describe the tension in a Kuhn segment subject to small distortion. The slight stretching of the bond length under shear flow at high shear rate (but within the limitation of $\Gamma y \ll 1$, of course) guarantees the linear force law. In fact, an unreasonably high shear rate must drive the segment stretched completely, and thus make the local microrelaxation in MC simulation very difficult. In experiment, it might result in the chain breaking due to extremely large tensions in chemical bonds. Hence, the extremely high shear rate is beyond the scope of this paper.

Besides the elongation of the flexible chain, the orientation of the flow birefringence is also crucial. According to literature,[27] the Rouse coil, which is spherical on average in zero field, has an ellipsoid shape under shear flow, whose long axis is oriented relative to the x axis with an angle of

$$\Theta=\frac{1}{2}\arctan\left(\frac{\text{const}}{\dot{\gamma}}\right), \tag{33}$$

in the xy plane. The constant is reversibly proportional to the longest relaxation time of the Rouse bead-spring model. Since the corresponding formula in Ref. 27 results from the conventional Rouse model in three dimensions, it is worth checking whether this relation still stands out for an improved Rouse model with excluded volume effect in two dimensions, irrespective of the concrete value of this constant. The MC simulation outputs are shown in Fig. 11, along with the fitted theoretical line based on Eq. (33). It appears that Eq. (33) is consistent with the ''computer-experiment'' measurements at low shear rate, but fails, to some extent, at high shear rate or in the nonlinear regime. The main difference is that the orientation angle is rapidly decreased to zero according to Eq. (33), while according to MC simulation, the orientation angle is decreased very slowly at high shear rate, which even implies the possibility with a positive, and therefore nonzero, asymptotic orientation angle. A similar phe-

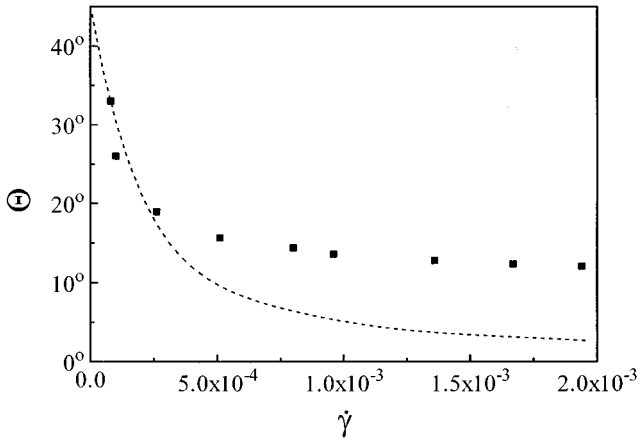

FIG. 11. Averaged orientation angle Θ as a function of shear rate $\dot{\gamma}$. The dashed line is the theoretical result from Eq. (33) with the constant, 0.000 18. (The simulation parameters are the same as those in Fig. 10.)

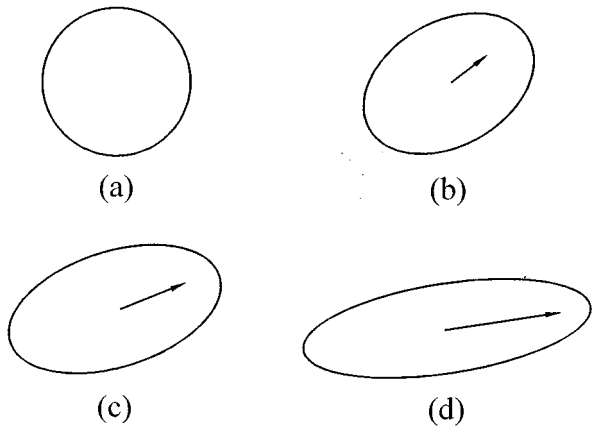

FIG. 12. Schematic presentation of the averaged chain shapes at steady state. (a) isotropic off the flow field; (b)–(d) anisotropic in the simple shear flow field with the flow direction along horizontal. The shear rate is increased from (b) to (d), which results in the order parameter increased and the orientation angle decreased, as indicated by marked arrows.

nomenon has been found for long time for LCs where the well-known Leslie angle describes the orientation of the LC director relative to the dimension of shear flow.[25,26] Pierleoni and Ryckaert[9] performed the molecular dynamics simulation of a single chain described by the bead-rod model and also found out the deformation and orientation of the chain under steady shear flow, but failed to point out the nonzero orientation angle at high shear rate. It might not be easy to confirm the nonzero orientation angle of flexible polymers at high shear rate because this angle is very small at very high shear rate. Nevertheless, it is nontrivial to conceptually understand that the asymptotic orientation angle of flexible polymers might not be zero with shear rate increased infinitely, just similar to rigid molecules. This viewpoint should be further confirmed in the future.

Based on Figs. 10 and 11, we can easily describe the change of the averaged chain shapes under shear flow as schematically presented in Fig. 12. The chain shape is, off the flow field, spherical on average in the laboratory frame. The chain configuration is, however, elongated under shear flow and the orientation of the long axis is, from nearly $\pi/4$ at very low shear rate, decreased with increasing shear rate. Since the highly elongated configuration at very high shear rate is close to an anisotropic rod, the rheological properties of flexible polymers at high shear rate, such as pronounced flow birefringence, the nonzero orientation angle, and the shear thinning effect (which will be shown in the next section), might be, to some extent, similar to those of LC polymers.[25,26]

V. NONLINEAR RHEOLOGICAL BEHAVIORS

A. Statistics of stress tensor

The significant rheological parameters such as viscosity and first normal stress difference, which are conventionally measured in experiment, are determined by the stress tensor. In the classic viscoelastic theories such as Rouse theory, these macroscopic physical parameters are analytically related to the spectrum of relaxation time since the dynamics of a long macromolecular chain is described by the combination of different normal relaxation modes.[1–6] With the help of MC simulation,[12] the polymer dynamics derived from the Kramers potential has been wonderfully treated for the Rouse model. Corresponding research should depend on the analytical, or at least to say, definite relations between the stress tensor and the spectrum of relaxation time.[17] Unfortunately, the relations in the case of nonlinear viscoelasticity for any kind of flow fields remain unknown. Even for a Rouse model with SAWs, the modes are strongly mixing. Just as pointed out by Carmesin and Kremer,[14] the Rouse modes as defined for the RWs are not the normal modes for two-dimensional SAWs, although the Rouse theory is valid for the SAW chain to some extent.[28] So, in order to study the nonlinear viscoelasticity of chains with excluded volume effect, it is not sufficient to merely obtain the relaxation time (let alone that the statistics of the spectrum of relaxation time is very much time-consuming in computer simulation). In this paper, we obtain the macroscopic stress tensors of a single macromolecular chain and multiple chains by statistics directly from the chain CDFs embodied in dynamic MC simulation. Both linear and nonlinear regimes can be investigated in the simple shear flow achieved by the combination of our pseudopotential and the four-site model. The improvement of the study approach is absolutely nontrivial. Some preliminary results in two dimensions are presented here. Further investigation will be published as a separate paper.

Since the four-site model can be thought of as a series of connected Kuhn segments with the fluctuation of segment length, just as an entropy spring, we can, after neglecting the contribution from hydrodynamic interaction, follow the Kramers form of the stress tensor for the bead-spring model[1] as

$$\hat{\tau}=\hat{\tau}_0-n\left\langle \sum_{k=1}^{N-1}\mathbf{F}_k^{(c)}\mathbf{Q}_k\right\rangle+(N-1)nkT\hat{\delta}, \tag{34}$$

where $\hat{\tau}$ is the total stress tensor of the polymer solution, and the first, second, and third terms on the right side of Eq. (34) come from the contributions from the solvent, the tensions in entropy springs, and the momentum transport by beads, respectively. $\hat{\delta}$ is the second-rank unit tensor for the two-dimensional bead-spring model, the average $\langle\cdots\rangle$ is performed over different ensembles, n is the number density of chains with $n=n_p/V$ (n_p and V are the number of polymers and the volume), $\mathbf{Q}_k$ is the connector vector between the kth and $(k+1)$th beads

$$\mathbf{Q}_k=\mathbf{r}_{k+1}-\mathbf{r}_k, \tag{35}$$

which gives the location of each bead relative to the bead immediately preceding it in the chain. $\mathbf{F}_k^{(c)}$ is the constraint tension in the kth connector, namely, the elastic force of the $(k+1)$th bead exerted on the kth bead, and reads

$$\mathbf{F}_k^{(c)}=Hl_k\mathbf{Q}_k/|\mathbf{Q}_k|=kTK\mathbf{Q}_k, \tag{36}$$

where the relation of $l_k=|\mathbf{Q}_k|$ is used. The elastic constants H and K are expressed as in Eqs. (2b) and (2c). At this point, we can see that the entropy spring expression of the so-called bond fluctuation in the four-site model, along with Eq. (2), is a prerequisite of the available statistics of the stress tensor of macromolecular chains. Such an interpretation of the four-site model, and thus the statistical method of stress tensor in on-lattice MC simulation, has not been reported, to our knowledge. It seems necessary to mention that the SAW effect on the macroscopic stresses, which is significant according to literature,[29] has been inherently involved in the present statistic approach since the CDF is influenced strikingly by the excluded volume interaction in our simulation.

As usual, the reduced stresses are treated in theory. The stress tensor is thus rewritten as

$$\hat{\sigma}=\frac{\hat{\tau}-\hat{\tau}_0}{kT}=\frac{n_p}{V}\left[(N-1)\hat{\delta}-K\left\langle\sum_{k=1}^{N-1}\mathbf{Q}_k\mathbf{Q}_k\right\rangle\right] \tag{37}$$

in the unit of V_{MC}^{-1}, where V_{MC} is the unit volume in MC simulation and expressed as l_{MC}^2 in two dimensions. Equation (37) is the fundamental formula for statistics of the stress tensor of macromolecular chains described by the bond fluctuation model with the interpretation of an entropy spring or, generally speaking, a bead-spring model. It is valid both in two and three dimensions, both in RWs and SAWs, both on and off external field, and both in the linear and nonlinear regimes if the hydrodynamic contribution is neglected. The reduced shear stress can be obtained directly from, and is in fact equal to, the xy component of the stress tensor, σ_{xy}. The apparent viscosity is thus

$$\eta=\frac{\sigma_{xy}}{\dot{\gamma}}. \tag{38}$$

Its unit is $V_{\mathrm{MC}}^{-1}t_{\mathrm{MC}}$ in MC simulation and is not mentioned in the following discussion, for convenience. The reduced first normal stress difference N_1 and the first normal stress coefficient Ψ_1 in the unit of $V_{\mathrm{MC}}^{-1}t_{\mathrm{MC}}^2$ are expressed as

$$N_1=\sigma_{xx}-\sigma_{yy}, \tag{39a}$$

$$\Psi_1=\frac{N_1}{\dot{\gamma}^2}. \tag{39b}$$

The second normal stress coefficient, Ψ_2, loses definition in two dimensions. The functions η and Ψ_1 are so important as to be named as viscometric functions or materials functions. By the novel on-lattice MC simulation approach put forward in the present paper, we can obtain the material functions of flexible macromolecular chains subject to simple shear flow in both the Newtonian and non-Newtonian regimes.

B. Shear-rate dependence of material functions

For most polymers, irrespective of flexible macromolecules or rigid ones, all material functions vary with $\dot{\gamma}$. So, polymers are a typical kind of non-Newtonian and more complicated, nonlinear viscoelastic fluid. In spite of the fact that a majority of polymeric solutions and the melts of industrial importance exhibit nonlinear viscoelasticity when subject to a deformation of reasonably high shear rate, neither the Rouse theory nor the Zimm theory describe the shear-rate-dependent viscometric functions of polymeric solutions, although the hydrodynamic interaction is involved in the latter molecular theory. Both Rouse and Zimm theories deal with a single chain.

The nonlinear viscoelasticity of multiple chains observed widely in experiment is, however, revealed in our on-lattice MC simulation (Fig. 13). The shear thinning effect at reasonably high shear rate is reproduced by Fig. 13 rather well. According to the rheological behaviors with shear rate increased, Fig. 13 can be roughly divided into two regimes: a Newtonian regime at low shear rate where the shear stress increases almost linearly with shear rate [Fig. 13(a)] and thus the viscosity is almost a constant [Fig. 13(b)]; and the non-Newtonian regime at medium shear rate or relatively high shear rate where the shear stress is not proportional to shear rate [Fig. 13(a)] and the viscosity strongly depends on the shear rate [Fig. 13(b)]. The second Newtonian regime, which has been observed in many polymeric fluids at higher shear rate,[30] is missed due to the limitation of $\Gamma y\ll 1$ in our MC simulation.

It is the privilege of our MC simulation to study the relation between the microscopic conformations of macromolecules and macroscopic rheological behaviors of polymers since both of them can be obtained independently. Comparison of Fig. 13 to Figs. 10 and 11 clearly reveals that the transition from Newtonian regime to non-Newtonian regime is closely related to the chain stretching and orientation.

Normal stress difference is another significant rheological parameter, which describes especially the fluid elasticity and accounts for the well-known extruded swelling (Barus effect), the rod climb-up (Weissenberg effect), and melt fracture effects in polymer processing.[30] The nonzero normal stress difference is reproduced (Fig. 14) and shows shear-rate

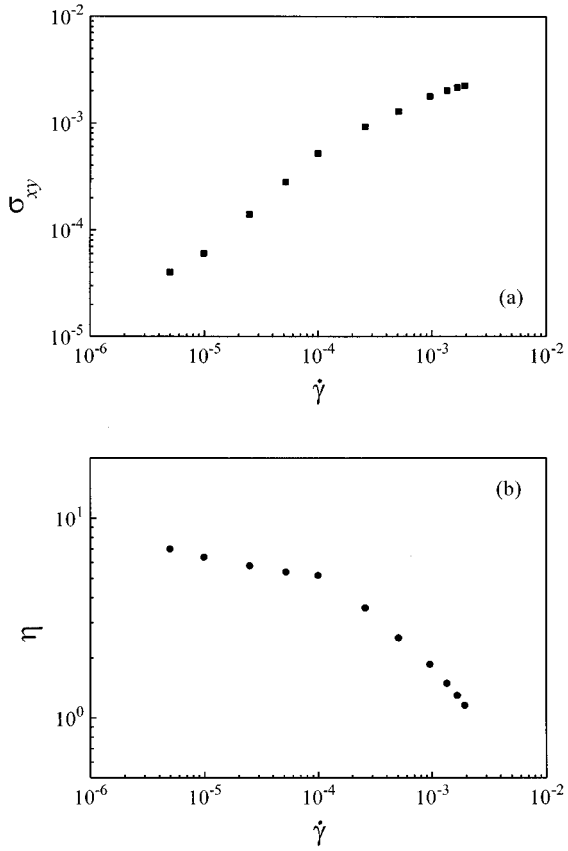

FIG. 13. (a) Reduced shear stress σ_{xy} and (b) corresponding reduced apparent viscosity η as a function of shear rate $\dot{\gamma}$. (The simulation parameters are the same as those in Fig. 10.)

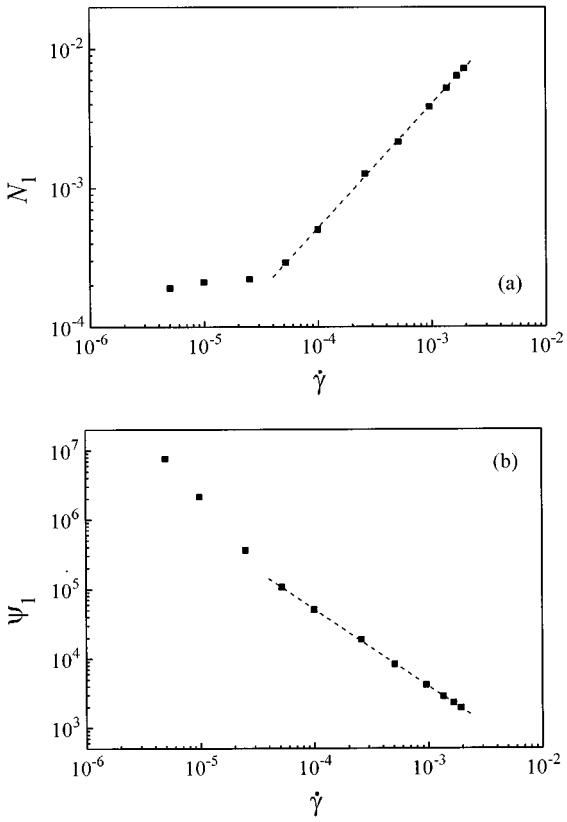

FIG. 14. (a) Reduced first normal stress difference N_1 and (b) its coefficient Ψ_1 as a function of shear rate $\dot{\gamma}$. The dashed lines are the fitted results with $N_1 \propto \dot{\gamma}^{0.9}$ and $\Psi_1 \propto \dot{\gamma}^{-1.1}$. (The simulation parameters are the same as those in Fig. 10.)

dependence for our free-draining bead-spring model with excluded volume effect. This phenomenon is missed in the original Rouse model although it is very popular in polymers. The improvement in our work is, in our opinion, mainly due to the permission of the nonlinear deformation of the CDF of macromolecular chains rather than the consideration of excluded volume effect. The quantities of the simulated first normal stress differences are with similar orders of the corresponding shear stress at the same shear rate within the regime of medium shear rate (Figs. 13 and 14), which is in accord with the experimental observations.[30] It is found in experiment that at higher shear rate, N_1 becomes much larger than σ_{xy}, and this causes many interesting unsteady phenomena, such as melt fracture. This unsteady phenomenon is difficult to simulate due to the limitation of shear rate in our MC approach. In order to shed light on the molecular origin of the nonzero normal stress difference and the transition from Newtonian regime to non-Newtonian regime, we especially show the associated change of chain configuration in Fig. 15, where the x and y components of mean square radius of gyration, along with the S_G^2 itself, are plotted as a function of shear rate $\dot{\gamma}$. Figure 15 is slightly different from Fig. 10(a), because S_x^2 and S_y^2 are determined by both the order parameter O shown in Fig. 10(b) and the orientation angle Θ shown in Fig. 11. If the orientation of the chain configuration is nearly along $\pi/4$, for instance, at low shear rate, the difference between S_x^2 and S_y^2 may be very small even if the order parameter can not be neglected. Figure 14 is, including the transition point, extremely consistent with Fig. 15. So it is very convincing that the difference between the xx and yy component of the stress tensor arises directly from that between the xx and yy components of correspond-

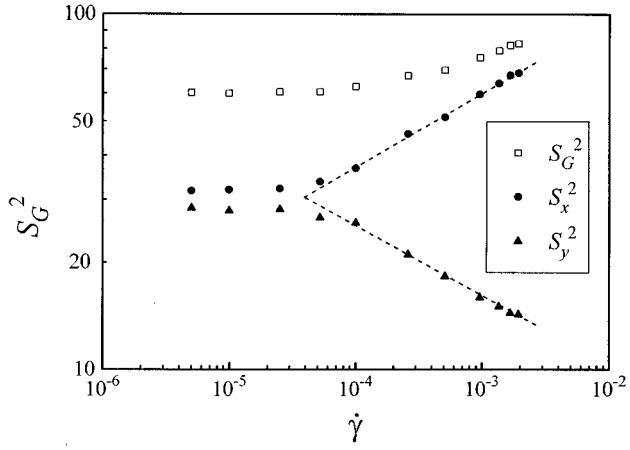

FIG. 15. The x and y components of mean square radius of gyration, S_x^2 and S_y^2 along with the whole mean square radius of gyration, S_G^2 as a function of shear rate $\dot{\gamma}$. The dashed lines are the fitted results with $S_x^2 \propto \dot{\gamma}^{0.2}$ and $S_y^2 \propto \dot{\gamma}^{-0.2}$. (The simulation parameters are the same as those in Fig. 10.)

ing tensor of radius of gyration. It is clear that the normal stress difference originates from the Brownian driving force to restore the most probable distribution in the quiescent state from the deformed CDF due to symmetry breaking flow, or equivalently, arises from the anisotropy of the entropy elasticity of every chain for flexible macromolecules under flow.

In many polymers, the shear-rate dependent rheological parameters obey the power law at high shear rate within some range. The power law is satisfied rather well in our MC simulation (Fig. 14) with

$$N_1 \propto \dot{\gamma}^{\alpha}, \tag{40a}$$

$$\Psi_1 \propto \dot{\gamma}^{\alpha-2}. \tag{40b}$$

We have also found out the power law in the change of chain shape (Fig. 15),

$$S_x^2 \propto \dot{\gamma}^{\beta_1}, \tag{41a}$$

$$S_y^2 \propto \dot{\gamma}^{-\beta_2}. \tag{41b}$$

The simulation outputs show that $\beta_1 = \beta_2$ in two dimensions (Fig. 15). Similar scaling law exists in the shear rate dependence of viscosity (Fig. 13), but is not as striking as that of the first normal stress difference. The exponent for the scaling relation between η and $\dot{\gamma}$ (Fig. 13) decreases, if it exists, with increased shear rate, which is consistent with some experimental observations.[1,30] To compare these exponents with the experimental measurements in detail is, of course, a task for our MC simulation in three dimensions and is not discussed here.

C. Chain-length dependence of zero-shear viscosity

In most polymeric solutions and melts, the viscosity is independent on shear rate at sufficiently low shear rate. The zero-shear viscosities η_0 of concentrated polymer solutions, and of the melts of linear polymers, are proportional to the molecular weight M or chain length below a critical value, whereas above this critical value it increases rapidly and become proportional to $M^{3.4}$.[30] This phenomenon is explained by the topological effect.[1–3] The topological effect is not involved in the chain dynamics in two dimensions even though the excluded volume effect has been taken into account completely in the four-site model. Nevertheless, the examination of the chain-length dependence of zero-shear viscosity is meaningful in its own right.

First, we studied the rheological behaviors in dilute solution for a single SAW chain for comparison with Rouse theory. For dilute polymeric solution, the intrinsic viscosity $[\eta]$ should be used to check the scaling law between viscosity and molecular weight. According to Eqs. (37) and (38), the stress of the polymeric solution has been subtracted by the contribution of solvent. So the intrinsic viscosity $[\eta]$ must be proportional to the ratio of the zero-shear viscosity η_0 to the number concentration of the segment, c with $c = n(N-1)$. For convenience, we define an effective intrinsic viscosity as

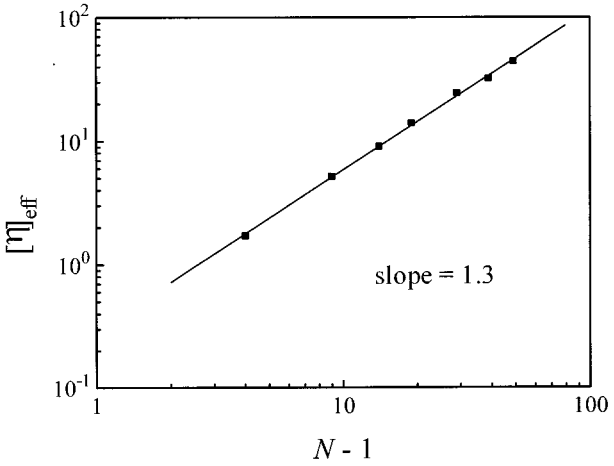

FIG. 16. The effective intrinsic viscosity $[\eta]_{\text{eff}}$ in dilute solution as a function of chain length $N-1$. (Single chain; $L_x \times L_y = 200 \times 200$; in statistics of viscosity at any shear rate for any chain length, 20 independent runs are averaged and for each run, 800 000 MC cycles are averaged after 100 000 MC cycles under shear.)

$$[\eta]_{\text{eff}} = \lim_{c \to 0} \frac{\eta_0}{c} \tag{42}$$

in the unit of t_{MC}. The simulation outputs (Fig. 16) are, to some extent, consistent with the prediction of Rouse theory, $[\eta] \propto (N-1)$, where the free-draining bead-spring model is analyzed without excluded volume effect in three dimensions.[1–3] The deviation of the component, 1.3 in Fig. 16 from 1 in Rouse theory,[1–3] is not explicitly known. We guess that it maybe comes from three origins: one is the SAW effect and the different dimensionality; the other might rely on the possibility that the constraint from upper and lower hard walls is more striking for a long chain than for a short chain; the last one might be due to the low signal-noise-ratio in statistics of zero-shear viscosity from the asymptotic behaviors of apparent viscosities at low shear rates.

The counterpart in the concentrated solution with the occupied volume fraction $\varphi = 0.5$ is shown in Fig. 17. Corresponding scaling law of the dynamic behavior (Fig. 17) is similar to that in the dilute solution (Fig. 16), which reflects some characteristics of chain dynamics in two dimensions. Since the attrition rate rises rapidly as the system density increased, it is not realistic to perform simulation for an over dense system with very high volume fraction such as $\varphi > 0.9$. Fortunately, as examined by Binder *et al.*,[16] an occupied volume fraction with $\varphi = 0.5$ is high enough for us to regard the corresponding system as in the bulk state. So, the present simulation approach is very efficient and is ready to investigate the condensed-state properties of polymers.

VI. CONCLUDING REMARKS

This paper extends the on-lattice MC method to simulate, for the first time, the simple shear flow of SAW macromolecular chains and to investigate the corresponding non-

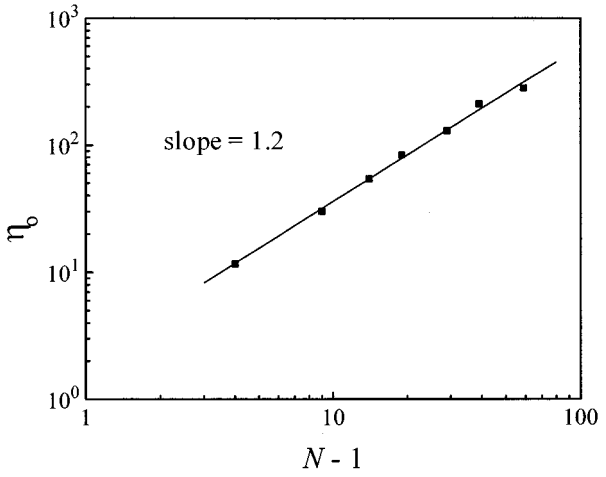

FIG. 17. Zero-shear viscosity η_0 in concentrated solution as a function of chain length $N-1$. ($\varphi=0.5$; $L_x\times L_y=120\times 120$; in statistics of the viscosity at any shear rate for any chain length, 10 independent runs are averaged and for each run, 20 000 MC cycles are averaged after 20 000 MC cycles under shear. Before shearing is performed in the computer, 400 000 MC cycles are made in zero field to achieve the equilibrium random initial state.)

linear chain dynamics and viscoelasticity by introducing a pseudopotential to describe the flow field with the four-site lattice model. This pseudopotential makes sense only for the potential difference associated with each local microrelaxational movement of a bead in the chain defined by the four-site model and bond fluctuation approach. The free-draining bead-spring model is thus investigated at low and medium or relatively high shear rate. As the first paper of a corresponding series, the pseudopotential is checked in detail here. Some simulation outputs in two dimensions are presented to confirm this novel approach, and to demonstrate the simulated nonlinear viscoelasticity of both a single SAW chain and multiple chains subject to a simple shear flow.

The simulated velocity profile is greatly satisfied with the requirement of the simple shear flow and with a nearly constant shear rate unless the shear rate is unreasonably high. The simulated results are consistent with the associated analysis based on the importance sampling method, especially the Glauber dynamics method. The chain tumbling is observed in the simulation of a single chain. The stretching and orientation of flexible chains are confirmed in computer experiment. The shear stress and first normal stress difference are obtained by statistics according directly to the simulated CDFs at low and relatively high shear rates. The material functions (apparent viscosity and first normal stress coefficient) show shear rate dependence at high shear rate, which is, in turn, explained by the large chain deformation on the microscopic origin. Both Newtonian regime and non-Newtonian regime are found in our on-lattice MC simulation. The nonlinear rheological behaviors revealed in MC simulation agree rather well with the experimental observations in literature for most polymers. The chain-length dependence of zero-shear viscosity can be reasonably explained by the present linear viscoelastic theory, to some extent.

The molecular theories of chain dynamics and viscoelasticity of polymers at hand can be, in our opinion, roughly divided into two fashions: one is the Rouse–Zimm fashion, the other is the deGennes–Edwards fashion, although many others have contributed to this fascinating field.[1–4,30–36] Unfortunately, these two kinds of theories can not be combined into one unified analytical theory at the present time. The novel simulation approach put forward in the present paper might shed light on this problem in the future, even though the computer simulation can not replace both experiment and analytical theory. This approach is able to obtain the CDFs of polymers in both Newtonian regime and non-Newtonian regime *by importance sampling method* and therefore, it is, in computer simulation, unnecessary to know the exact analytical expressions of those CDFs, which are, in fact, unknown for SAW chains in the non-Newtonian regime up to now. Thanks to Kremer *et al.*,[14–18] the intersection of different segments is forbidden in the bond fluctuation approach. As a result, the SAW has been completely taken into account in the four site lattice model and thus, the entanglement effect under shear flow can be studied in the nonlinear regime by our MC simulation in three dimensions after combination of the pseudopotential and the bond fluctuation model. No further assumption should be made at all when we extend the simulation approach for a single chain to that for multiple chains. To study SAW is the privilege of MC and is especially easy in the simulation on lattice. Even simulating multiple SAW chains does not bring about much difficulty within the realistic running time for the on-lattice MC approach. Therefore, both the dilute solution and concentrated solution of SAW polymeric chains can be investigated by one unified simulation method. The other advantage of the present approach is that by statistics of the sampled CDF, we can independently determine the deformed chain conformation under flow field, and meanwhile, ''measure'' the stresses and corresponding rheological parameters which are available in experimental measurement. The relationship between the microscopic structures and macroscopic properties can thus be revealed. The main drawback of our approach is that the hydrodynamic interaction is not involved, whereas in some other simulation approaches such as Brownian dynamics simulation, the hydrodynamic interaction is involved.[37] Nevertheless, considering again that the on-lattice MC simulation is rather efficient compared to the off-lattice simulation approaches, and is available even on a personal computer, we would like to promise that the novel approach to simulate the shear flow might be helpful for explaining many complicated rheological behaviors of polymeric fluids on the molecular level.

ACKNOWLEDGMENTS

This research was supported by NSF of China, The Foundation for Young Scientists from The State Science and Technology Commission of China (STCC), The Doctoral Programme Foundation of Institution High Education from

the State Education Commission (SEDC) of China, and The National Key Projects for Fundamental Research ''Macromolecular Condensed State'' from STCC.

[1] R. B. Bird, O. Hassager, R. C Armstrong, and C. F. Curtiss, *Dynamics of Polymeric Liquids* (Wiley, New York, 1977).
[2] P. G. deGennes, *Scaling Concepts in Polymer Physics* (Cornell University Press, Ithaca, New York, 1979).
[3] M. Doi and S. F. Edwards, *The Theory of Polymer Dynamics* (Clarendon, Oxford, 1986).
[4] P. J. Flory, *Principles of Polymer Chemistry* (Cornell University Press, Ithaca, 1953).
[5] P. E. Rouse, J. Chem. Phys. **21**, 1272 (1953).
[6] B. H. Zimm, J. Chem. Phys. **24**, 269 (1956).
[7] A. Baumgartner, in *Applications of the Monte Carlo Method in Statistical Physics*, edited by K. Binder (Springer, Berlin, 1984).
[8] K. Kremer and K. Binder, Comput. Phys. Rep. **7**, 259 (1988).
[9] C. Pierleoni and J. P. Ryckaert, Macromolecules **28**, 5097 (1995).
[10] (a) T. W. Liu, J. Chem. Phys. **90**, 5826 (1989); (b) P. J. Dotson, *ibid*. **79**, 5730 (1983); (c) H. C. Ottinger, *ibid*. **84**, 1850 (1986).
[11] H. A. Kramers, J. Chem. Phys. **14**, 415 (1946).
[12] H. L. Frisch, N. Pistoor, A. Sariban, K. Binder, and S. Fesjian, J. Chem. Phys. **89**, 5194 (1988).
[13] J. Ding, G. Xu, and Y. Yang, Abstracts of IUPAC International Symposium on Macromolecular Condensed State, **111** (Beijing, 1996).
[14] I. Carmesin and K. Kremer, Macromolecules **21**, 2819 (1988).
[15] H. P. Deutsch and K. Binder, J. Chem. Phys. **94**, 2294 (1991).
[16] H. P. Wittmann, K. Kremer, and K. Binder, J. Chem. Phys. **96**, 6291 (1992).
[17] W. Paul and K. Binder, Polym. Prepr. **33**, 535 (1992).
[18] J. Wittmer, W. Paul, and K. Binder, Macromolecules **25**, 7211 (1992).
[19] P. H. Verdier and W. H. Stockmayer, J. Chem. Phys. **36**, 227 (1962).
[20] R. G. Larson, L. E. Scriven, and H. T. Davis, J. Chem. Phys. **83**, 2411 (1985).
[21] R. I. Tanner and J. Stehrenberger, J. Chem. Phys. **55**, 1958 (1971).
[22] N. Metropolis, A. W. Rosenbluth, M. N. Rosenbluth, A. H. Teller, and E. Teller, J. Chem. Phys. **21**, 1087 (1953).
[23] R. J. Glauber, J. Math. Phys. **4**, 294 (1963).
[24] G. Xu, J. Ding, and Y. Yang, J. Fudan Univ. Nat. Sci. (to be published) (in Chinese).
[25] J. Ding and Y. Yang, Rheol. Acta **33**, 405 (1994).
[26] J. Ding and Y. Yang, Polymer **37**, 5301 (1996).
[27] N. Pistoor and K. Binder, Colloid Polym. Sci. **266**, 132 (1988).
[28] (a) M. Dial, K. S. Crabb, and J. Kovac, Macromolecules **18**, 2215 (1985); (b) J. P. Downey, C. C. Crabb, and J. Kovac, *ibid*. **19**, 2202 (1986).
[29] (a) M. Fixman, J. Chem. Phys. **95**, 1410 (1991); (b) J. Gao and J. H. Weiner, Macromolecules **25**, 3462 (1992).
[30] C. D. Han, *Rheology in Polymer Processing* (Academic, New York, 1976).
[31] F. Bueche, J. Chem. Phys. **22**, 603 (1954).
[32] M. Fixman, J. Chem. Phys. **45**, 785 (1966).
[33] J. G. Kirkwood, *Macromolecules* (Gordon and Breach, New York, 1967).
[34] J. D. Ferry, *Viscoelastic Properties of Polymers* (Wiley, New York, 1970).
[35] M. Fixman and W. H. Stockmayer, Annu. Rev. Phys. Chem. **21**, 407 (1970).
[36] H. Yamakawa, *Modern Theories of Polymer Solutions* (Harper & Row, New York, 1971).
[37] M. Fixman, J. Chem. Phys. **78**, 1594 (1983).